IEEE Access
Multidisciplinary | Rapid Review | Open Access Journal

Received May 31, 2017, accepted June 21, 2017, date of publication July 11, 2017, date of current version July 31, 2017.

Digital Object Identifier 10.1109/ACCESS.2017.2725450

Robust Adaptive Beamforming Using Noise Reduction Preprocessing-Based Fully Automatic Diagonal Loading and Steering Vector Estimation

YUXUAN KE, CHENGSHI ZHENG, (Senior Member, IEEE), RENHUA PENG, AND XIAODONG LI

Institute of Acoustics, University of Chinese Academy of Sciences, Beijing 100190, China
Acoustics and Information Technology Laboratory, Shanghai Advanced Research Institute, Chinese Academy of Sciences, Shanghai 201210, China

Corresponding author: Chengshi Zheng (cszheng@mail.ioa.ac.cn)

This work was supported by the National Science Fund of China under Grant 61571435 and Grant 61302126.

ABSTRACT Diagonal loading provides a powerful and effective way to improve the robustness of the standard Capon beamformer. Several parameter-free robust adaptive beamformers (RAB) are considered in this paper. We reveal that the performances of them have somewhat degradation when the number of snapshots or that of sensors is large. To solve this problem, we emphatically study the well-known generalized linear combination-based method, the performance of which may degrade severely when the number of sensors increases, and propose a novel parameter-free technique, which is a combination of noise reduction preprocessing technique and truncated minimum mean square error criterion. As most of the parameter-free RAB techniques are very sensitive to the desired signal steering vector mismatch, this paper further proposes to construct a series connection between these RAB techniques and a steering vector estimation (SVE) method, where the SVE is implemented by a convex optimization technique. Simulation results show that the proposed method can achieve a promising performance in comparison with the competing methods.

INDEX TERMS Diagonal loading, robust adaptive beamforming, parameter-free, steering vector estimation.

I. INTRODUCTION

The standard Capon beamformer (SCB) is an optimal spatial filter with remarkable resolution and interference suppression capability [1]. However, it is very sensitive to the imprecise knowledge of the true covariance matrix and the mismatch of the steering vector of signal-of-interest (SOI). In the last half century, many robust adaptive beamformers (RAB) have already been proposed to improve the robustness of SCB. They can be roughly classified into four categories: diagonal loading method [2]–[5], uncertainty set-based method [6]–[11], eigenspace-based method [12]–[14], and interference-plus-noise covariance matrix reconstruction-based method [15]–[18].

Diagonal loading is one of the most widely used RAB method, where a scaled identity matrix is injected into the sample covariance matrix according to some rules [2]. Most of the conventional diagonal loading methods are user parameter dependent. For example, the norm constrained Capon beamforming is a frequently used conventional diagonal loading method, whose the diagonal loading level is determined by the user parameter upper bound of the square of the weight vector norm [2]. In recent decades, the uncertainty set-based robust adaptive beamformers have been proposed, such as the worst-case performance optimization beamformer [7], the linear programming beamformer [8], and the distributional robust chance-constrained beamformer [9]. They are proved equivalent to the diagonal loading method [6], and their corresponding diagonal loading level can be calculated by the user defined size of the uncertainty set of the array steering vector. Therefore, the conventional diagonal loading method and the uncertainty set-based diagonal loading method have the common problem that their diagonal loading level is uneasy to be determined beforehand.

Several parameter-free RAB techniques have been presented in the literature, including the Hoerl-Kennard-Baldwin (HKB) method [19], the general linear combination-based (GLC) method [20], the spatial matched filter-based (SMF) method [21], and the quadratically

constrained (QC) method [22]. HKB is based on the generalized sidelobe canceler formulation of SCB, which belongs to the family of the ridge regression Capon beamformer [23]. As has been pointed out in [20], HKB's performance degrades when the number of snapshots beyond a certain number, i.e., from hundreds to thousands times as many as the number of sensors. GLC is a shrinkage-based beamformer which is usually utilized in knowledge-aided space-time adaptive processing [24]–[26], where it estimates the true covariance matrix in the sense of minimum mean square errors (MMSE). However, the performance of GLC degrades when the number of sensors is relatively large, i.e., from tens to hundreds times as many as the number of directional signals. The output power of the spatial matched filter associated with the SOI is chosen as the diagonal loading level for the SMF method, which has a low computational complexity [21]. However, as the diagonal loading level of SMF fluctuates mildly around a constant, in the scenario of large number of snapshots, the diagonal loading level of SMF may be too large that will result in the reduction of null depth of the beamformer, while in the scenario with small number of snapshots, the diagonal loading level may be too small that will affect the robustness of this technique. QC is based on a nonconvex quadratically constrained optimization technique, where the diagonal loading factor is introduced in by an iterative algorithm [22]. We reveal that QC has some limitations on the desired uncertainty range of DOA, the array geometry and the allowable maximum number of sensors.

As the scenario of large number of sensors is popular recently [27]–[33], this paper focuses on improving the performance of SCB for a large array. We study how the number of sensors will affect the MMSE estimator in the GLC technique and thus present a novel fully automatic diagonal loading method which estimate the true covariance matrix by combining noise reduction preprocessing with truncated MMSE (NRP-TMMSE) criterion, where the noise reduction can be implemented by the least-square-estimate (LSE) method [34] and the multichannel wiener filtering (MWF) method [35] with a roughly estimation of the number of directional signals.

The mentioned parameter-free RAB techniques all focus on the covariance matrix estimate except QC, which consider an uncertainty set that constrains the steering vectors with a desired uncertainty range of DOA. As a consequence, HKB, GLC, SMF, and NRP-TMMSE are all somewhat sensitive to both the DOA mismatch and the sensor position perturbations. To further solve this problem, a joint estimation of covariance matrix and steering vector has been proposed [36], where the estimation of covariance matrix is implemented by GLC and the steering vector is estimated using the method proposed by the literature [10]. As a result, this method retains the drawbacks of GLC and the estimation of steering vector relies on the precise knowledge of the number of directional signals. Differently, this paper proposes a new RAB technique by constructing a series connection between NRP-TMMSE and a steering vector estimation (SVE) method that is based on a convex optimization technique [11]. The only prior information used in the corresponding SVE method is the imprecise knowledge of the angular sector of the desired signal and array geometry, resulting in a high robustness of the proposed NRP-TMMSE-SVE.

Numerous simulation results show that NRP-TMMSE-SVE has better performance in terms of the robustness and the output signal-to-interference-noise ratio (SINR) in most cases when comparing with other diagonal loading methods, especially when the number of sensors is relatively large (from tens to hundreds times as many as the number of directional signals), and that of snapshots is relatively small (less than twice as many as the number of sensors). Besides, the performance of NRP-TMMSE-SVE is robust to the imprecise estimation of the number of signals.

The contributions of our work are briefly listed as follows.

i) Asymptotic analysis on the performances of the existing non-parameter RAB techniques are demonstrated in two limiting cases (the number of snapshots/sensors trends to be infinite). This analysis shows that the tendency of the diagonal loading levels of these techniques is somewhat unreasonable when considering covariance matrix uncertainty under these two assumptions.
ii) To improve the performance of GLC in the case with a large number of sensors, we propose a NRP-TMMSE method, which combines the noise reduction preprocessing algorithm with a proposed truncated MMSE criteria, and validate the feasibility of the LSE method [34] as well as the MWF method [35] in the noise reduction preprocessing procedure.
iii) A SVE method based on convex optimization technique [11] is proposed to be connected with NRP-TMMSE as well as the existing RAB techniques, which can improve the robustness of these techniques against the steering vector mismatch.

II. SIGNAL MODEL AND PROBLEM FORMULATION

We consider D far-field narrowband signals impinging on an array of M ($M > D$) omnidirectional sensors. Although the cases with multipath propagation has been considered in array processing recently, e.g., see [21], the unipath propagation is widely assumed in this field, e.g., [19], [20], [22], and [36]. In this paper, we only consider the case with unipath propagation. Thus, nth snapshot of the received signal can be written as a vector $\mathbf{x}(n) \in \mathbb{C}^{M\times 1}$, which is

$$\mathbf{x}(n) = \sum_{d=0}^{D-1} \mathbf{a}_d s_d(n) + \mathbf{n}(n), \tag{1}$$

where $s_d(n)$ with ($d = 0, 1, \ldots, D-1$) denote the D directional narrowband signals. We assume that $d = 0$ corresponds to the SOI and $d = 1, 2, \ldots, D-1$ correspond to the interferences. $\mathbf{a}_d \in \mathbb{C}^{M\times 1}$ is the steering vector of the signal s_d with $\|\mathbf{a}_d\|^2 = M$, $\mathbf{n}(n) \in \mathbb{C}^{M\times 1}$ is the additive noise vector.

The true covariance matrix can be expressed as

$$\mathbf{R}_x = E\left\{\mathbf{x}(n)\mathbf{x}^H(n)\right\} = \sigma_0^2\mathbf{a}_0\mathbf{a}_0^H + \mathbf{Q}, \tag{2}$$

where $E\{\cdot\}$ denotes the expectation operator, the superscript H denotes Hermitian transpose, σ_0^2 denotes the power of the SOI, and $\mathbf{Q}$ is the interference-plus-noise covariance matrix. SCB is formulated so as to select a weight vector that minimizes the array output power by using the following linearly constrained quadratic equations:

$$\min_{\mathbf{w}} \mathbf{w}^H\mathbf{R}_x\mathbf{w}, \quad s.t.\ \mathbf{w}^H\mathbf{a}_0 = 1. \tag{3}$$

If the steering vector of the SOI, $\mathbf{a}_0$, and the true covariance matrix, $\mathbf{R}_x$, are accurately known, the optimal weight vector and its corresponding optimal output SINR can be, respectively, given by

$$\mathbf{w}_{\text{opt}} = \frac{\mathbf{R}_x^{-1}\mathbf{a}_0}{\mathbf{a}_0^H\mathbf{R}_x^{-1}\mathbf{a}_0}, \tag{4}$$

$$\begin{aligned}\text{SINR}_{\text{opt}} &= \frac{\sigma_0^2\left|\mathbf{w}_{\text{opt}}^H\mathbf{a}_0\right|^2}{\mathbf{w}_{\text{opt}}^H\mathbf{Q}\mathbf{w}_{\text{opt}}} \\ &= \sigma_0^2\mathbf{a}_0^H\mathbf{Q}^{-1}\mathbf{a}_0.\end{aligned} \tag{5}$$

In practical applications, the true covariance matrix $\mathbf{R}_x$ is unknown, which needs to be substituted by the sample covariance matrix, given by:

$$\widehat{\mathbf{R}}_x = \frac{1}{N}\sum_{n=1}^{N}\mathbf{x}(n)\mathbf{x}^H(n), \tag{6}$$

where N is the number of snapshots. The estimated weight vector and the output SINR of SCB are, respectively, given by

$$\mathbf{w}_{\text{SCB}} = \frac{\widehat{\mathbf{R}}_x^{-1}\mathbf{a}_0}{\mathbf{a}_0^H\widehat{\mathbf{R}}_x^{-1}\mathbf{a}_0}, \tag{7}$$

$$\text{SINR}_{\text{SCB}} = \frac{\sigma_0^2\left|\mathbf{w}_{\text{SCB}}^H\mathbf{a}_0\right|^2}{\mathbf{w}_{\text{SCB}}^H\mathbf{Q}\mathbf{w}_{\text{SCB}}}. \tag{8}$$

As we know, the true covariance matrix can not be estimated accurately due to limited available data samples. As N increases, $\widehat{\mathbf{R}}_x$ can converge to $\mathbf{R}_x$, and the output SINR will approach SINR_{opt}. Unfortunately, the convergence rate of SCB is very slow, especially in the presence of SOI. Therefore, even in the absence of steering vector mismatch, the performance of SCB can degrade substantially when the number of snapshots is relatively small [2].

III. TYPICAL PARAMETER-FREE RAB TECHNIQUES

To improve the performance of SCB, many diagonal loading methods have been proposed and widely used [2]–[5], [19]–[22]. Supposing ρ is the corresponding diagonal loading level, the weight vector can be expressed as

$$\mathbf{w}_{\text{DL}} = \frac{(\widehat{\mathbf{R}}_x + \rho\mathbf{I})^{-1}\mathbf{a}_0}{\mathbf{a}_0^H(\widehat{\mathbf{R}}_x + \rho\mathbf{I})^{-1}\mathbf{a}_0}. \tag{9}$$

When $\rho = 0$, (9) reduces to SCB. Conversely, when $\rho \to \infty$, it becomes the delay-and-sum beamformer due to $\mathbf{w}_{\text{DL}} \to \mathbf{a}_0/M$ [2].

Because ρ has a significant impact on improving the performance of SCB [3], it is always a hot topic to choose an optimal diagonal loading level according to the given data.

A. HKB METHOD

HKB is a parameter-free robust beamformer [19], whose weight vector has the following form:

$$\mathbf{w} = \frac{\mathbf{a}_0}{M} - \mathbf{B}\eta, \tag{10}$$

where $\mathbf{B} \in \mathbb{C}^{M\times(M-1)}$ is the blocking matrix, with $\mathbf{B}^H\mathbf{a}_0 = \mathbf{0}$ and $\mathbf{B}^H\mathbf{B} = \mathbf{I}$. The blocking matrix is not unique, and its columns can be calculated as the eigenvectors corresponding to the $M-1$ non-zero eigenvalues of $\mathbf{I} - \mathbf{a}_0\mathbf{a}_0^H/M$. By introducing (10), (3) can be interpreted as a least-squares (LS) problem [19]. Let $\mathbf{X} = \widehat{\mathbf{R}}_x^{1/2}\mathbf{B}$ and $\mathbf{b} = \widehat{\mathbf{R}}_x^{1/2}\mathbf{a}_0/M$, then the LS problem can be expressed as

$$\begin{aligned}\min_{\eta}\left(\mathbf{B}\eta - \frac{\mathbf{a}_0}{M}\right)^H\widehat{\mathbf{R}}_x\left(\mathbf{B}\eta - \frac{\mathbf{a}_0}{M}\right) \\ = \min_{\eta}\|\mathbf{X}\eta - \mathbf{b}\|^2,\end{aligned} \tag{11}$$

where η can be estimated as

$$\hat{\eta} = (\mathbf{X}^H\mathbf{X})^{-1}\mathbf{X}^H\mathbf{b}. \tag{12}$$

Thus, the diagonal loading level of HKB can be calculated as [19]

$$\rho_{\text{HKB}} = \frac{(M-1)\hat{\sigma}^2}{\|\hat{\eta}\|^2}, \tag{13}$$

with

$$\hat{\sigma}^2 = \|\mathbf{X}\hat{\eta} - \mathbf{b}\|^2, \tag{14}$$

where $\|\cdot\|$ denotes the Frobenius norm of a matrix.

Finally, the weight vector of HKB can be written as

$$\mathbf{w}_{\text{HKB}} = \frac{(\widehat{\mathbf{R}}_x + \rho_{\text{HKB}}\mathbf{I})^{-1}\mathbf{a}_0}{\mathbf{a}_0^H(\widehat{\mathbf{R}}_x + \rho_{\text{HKB}}\mathbf{I})^{-1}\mathbf{a}_0}. \tag{15}$$

B. GLC METHOD

GLC is another parameter-free beamformer [20]. In this method, an estimate of $\mathbf{R}_x$ is a linear combination of the sample covariance matrix $\widehat{\mathbf{R}}_x$ and an identity matrix $\mathbf{I}$:

$$\widetilde{\mathbf{R}}_x = \alpha\widehat{\mathbf{R}}_x + \beta\mathbf{I}, \tag{16}$$

where $\widetilde{\mathbf{R}}_x$ is a positive semidefinite matrix ($\widetilde{\mathbf{R}}_x \geq 0$). α and β are the nonnegative shrinkage parameters which can be obtained by minimizing the mean square error of $\widetilde{\mathbf{R}}_x$, given by

$$\begin{aligned}\min_{\alpha,\beta}\left\{\text{MSE}(\widetilde{\mathbf{R}}_x)\right\} &= \min_{\alpha,\beta}E\left\{\|\widetilde{\mathbf{R}}_x - \mathbf{R}_x\|^2\right\} \\ &= \min_{\alpha,\beta}E\left\{\|\alpha\widehat{\mathbf{R}}_x + \beta\mathbf{I} - \mathbf{R}_x\|^2\right\}.\end{aligned} \tag{17}$$

By some mathematical derivations, the shrinkage parameters α and β can be obtained, which can be given by:

$$\alpha = \frac{\gamma}{\varepsilon + \gamma}, \tag{18}$$

$$\beta = \nu(1-\alpha) = \nu\frac{\varepsilon}{\varepsilon + \gamma}, \tag{19}$$

where $\varepsilon \triangleq E\{\|\widehat{\mathbf{R}}_x - \mathbf{R}_x\|^2\}$, $\gamma = \|\nu\mathbf{I} - \mathbf{R}_x\|^2$, and $\nu = \mathrm{tr}(\mathbf{R}_x)/M$, in which $\mathrm{tr}(\cdot)$ is the trace operator. In practice, $\mathbf{R}_x$ is unknown, [20] provided an effective way to estimate α and β without the knowledge of $\mathbf{R}_x$, which are denoted as $\hat{\alpha}$ and $\hat{\beta}$, respectively, herein. Assuming $\hat{\alpha} \neq 0$, the weight vector of GLC can be written as

$$\mathbf{w}_{\mathrm{GLC}} = \frac{\left(\widehat{\mathbf{R}}_x + \frac{\hat{\beta}}{\hat{\alpha}}\mathbf{I}\right)^{-1}\mathbf{a}_0}{\mathbf{a}_0^H\left(\widehat{\mathbf{R}}_x + \frac{\hat{\beta}}{\hat{\alpha}}\mathbf{I}\right)^{-1}\mathbf{a}_0}, \tag{20}$$

where $\hat{\beta}/\hat{\alpha}$ denoted as ρ_{GLC} is the diagonal loading level of GLC.

C. SMF METHOD

The diagonal loading level of SMF is empirically defined as [21]

$$\rho_{\mathrm{SMF}} = \bar{\mathbf{a}}_0^H\widehat{\mathbf{R}}_x\bar{\mathbf{a}}_0, \tag{21}$$

where, $\bar{\mathbf{a}}_0 = \mathbf{a}_0/\|\mathbf{a}_0\|$ is the normalized steering vector. The reason for defining this loading level is as follows.

The loading level of an effective diagonal loading method should satisfies the two conditions [3]: (a) the loaded noise eigenvalues are approximately equal, and (b) the loaded interference eigenvalues are minimally affected. Since the loading level given in (21) is actually the output power of the spatial matched filter, which contains three parts: the filtered noise power $\tilde{\sigma}_n^2$, signal power $\tilde{\sigma}_0^2$ and interference power $\tilde{\sigma}_d^2$, with $d = 1, \ldots, D-1$, ρ_{SMF} is usually much larger than the noise power. Thus, the condition (a) can be satisfied generally. As $\tilde{\sigma}_d^2$ will be at least 13 dB smaller than the input interference power σ_d^2 [37], with $d = 1, \ldots, D-1$, assuming that the desired signal power is much smaller than the interference power, then $\rho_{\mathrm{SMF}} \ll \sigma_d^2$, $d = 1, \ldots, D-1$, and the condition (b) is satisfied too. However, when the desired signal power is equal or larger than the interference powers, the condition (b) will not be satisfied, leading to the null depths reduction of the beampattern.

D. QC METHOD

The QC method is a simplified version of the uncertainty-based methods, which only constrains the steering vectors with a desired uncertainty range of DOA. Define the uncertainty range of DOA as $[\theta_1, \theta_2]$ herein, where $\theta_1 \leq \theta_0 \leq \theta_2$ and θ_0 is the impinging direction of SOI, to find a suboptimal solution, the optimization problem can be written as [22]

$$\min_{\mathbf{w},\phi,l_0\geq 1,l_1\geq 1} \quad \mathbf{w}^H\mathbf{R}_x\mathbf{w} \tag{22}$$

$$\text{subject to} \quad \mathbf{A}^H\mathbf{w} = \begin{pmatrix} l_0 \\ l_1\, e^{j\phi} \end{pmatrix}, \tag{23}$$

where, $\mathbf{A} = [\,\mathbf{a}(\theta_1)\ \mathbf{a}(\theta_2)\,]$, $\mathbf{a}(\theta_1)$ and $\mathbf{a}(\theta_2)$ are the steering vectors with directions θ_1 and θ_2, respectively. l_0, l_1, and ϕ are real numbers. If we let

$$\left(\mathbf{A}^H\mathbf{R}_x^{-1}\mathbf{A}\right)^{-1} = \begin{pmatrix} r_0 & r_2\, e^{j\mu} \\ r_1\, e^{-j\mu} & r_0 \end{pmatrix}, \tag{24}$$

where r_0, r_1, and r_2 are non-negative numbers, then l_0, l_1 can be calculated as

$$l_0 = \begin{cases} 1, & \frac{r_2}{r_0} \leq 1 \\ \frac{r_2}{r_0}, & \frac{r_2}{r_0} > 1, \end{cases} \quad l_1 = \begin{cases} 1, & \frac{r_2}{r_1} \leq 1 \\ \frac{r_2}{r_1}, & \frac{r_2}{r_1} > 1, \end{cases} \tag{25}$$

and ϕ can be chosen as $-\mu + \pi$. As the solution of the optimization problem can be obtained as

$$\mathbf{w}_{\mathrm{QC}} = \mathbf{R}_x^{-1}\mathbf{A}\left(\mathbf{A}^H\mathbf{R}_x^{-1}\mathbf{A}\right)^{-1}\begin{pmatrix} l_0 \\ l_1\, e^{j\phi} \end{pmatrix}, \tag{26}$$

The final QC beamformer can be obtained by substituting (24) and (25) into (26).

To avoid the zero between θ_1 and θ_2, the diagonal loading method is used to modify the objective function in an iterative way. The detailed procedure can be referred to in the literature [22].

Remarkably, this technique only works with an uniform linear array (ULA), and the desired uncertainty range of DOA must satisfy the inequality

$$|\sin\theta_2 - \sin\theta_1| \leq \frac{\lambda}{dM}, \tag{27}$$

where λ is the wavelength, and d is the inter-element space of sensors.

IV. ASYMPTOTIC ANALYSIS OF PARAMETER-FREE TECHNIQUES

In this section, we analyze the performance of the parameter-free techniques mentioned above in terms of their diagonal loading levels, where two limiting cases are considered that the number of snapshots N and the number of sensors M approach infinity. As the scenario of large number of sensors is popular recently [27]–[33], we emphatically analyze the case with a large value of M (from tens to hundreds times as many as the number of directional signals). Note that diagonal loading is introduced to improve the robustness of RAB against covariance matrix uncertainty, a proper diagonal loading level is expected to achieve a high output SINR.

A. IMPACT OF THE NUMBER OF SNAPSHOTS

On the one hand, when the number of snapshots N increases with a given number of sensors M, SCB tends to work optimally in the absence of steering vector mismatch, and thus the diagonal loading level should decrease. In a limiting

case, when the number of snapshots tends to be infinite, the theoretical diagonal loading level should be close to zero, however, the diagonal loading level of HKB tends to become infinite too [20]. This is because the numerator of ρ_{HKB} which represents the estimate SOI power will be as large as the true SOI power, while the denominator which is the solution of the LS problem (11) will decline to 0, resulting in a serious degradation of its performance, even worse than SCB.

The diagonal loading level of SMF tends to become a constant when the number of snapshots becomes infinite, due to that $\widehat{\mathbf{R}}_x$ is equal to $\mathbf{R}_x$, and the diagonal loading level given in (21) is exactly the output power of the spatial matched filter. If the input desired signal power is relatively large, ρ_{SMF} will be much larger than 0, leading to the null depths reduction of the beampattern. In addition, when the number of snapshots N is very small, i.e., less than M, the diagonal loading level of SMF is not large enough, which may also reduce its performance.

B. IMPACT OF THE NUMBER OF SENSORS

On the other hand, when the number of sensor M increases with a given number of snapshots N, the estimation uncertainty of the sample covariance matrix will increase when considering the Cramér-Rao bounds distance between $\widehat{\mathbf{R}}_x$ and $\mathbf{R}_x$ [38], thus a larger diagonal loading level is expected. The diagonal loading level of QC will satisfy the expected trend, because the number of iteration will also increase when M increases, followed by an increasing diagonal loading level. However, as shown in (27), the assumed uncertainty range of DOA will be very small as M approaches a large value [22], which may lead to the degradation of its robustness. In the meanwhile, the diagonal loading level of GLC will decrease as M increases. A proof is presented in this part to show this behavior.

From (18) and (19), the theoretical diagonal loading level of GLC can be calculated as

$$\rho_{\mathrm{o,GLC}} = \frac{\beta}{\alpha} = \nu\frac{\varepsilon}{\gamma}. \tag{28}$$

We focus on analyzing the change tendency of the three parameters ν, ε and γ as M increases with a given number of snapshots N.

Supposing the number of sensors is a variable, when it is equivalent to M, we let $\mathbf{R}_M$ denote the true covariance matrixes and rewrite (2) as

$$\mathbf{R}_M = \sum_{d=0}^{D-1}\sigma_d^2\mathbf{a}_d\mathbf{a}_d^H + \sigma_n^2\mathbf{I}_M, \tag{29}$$

where $\sigma_d^2\,(d = 0,\ldots,D-1)$ is the power of the dth directional signal, σ_n^2 is the power of the white complex Gaussian random process, and $\mathbf{I}_M$ is the unit matrix with the size $M \times M$, then the parameter ν can be calculated as

$$\nu = \frac{\mathrm{tr}(\mathbf{R}_M)}{M} = \frac{M(\sum_{d=0}^{D-1}\sigma_d^2 + \sigma_n^2)}{M} = \sum_{i=0}^{D-1}\sigma_d^2 + \sigma_n^2, \tag{30}$$

thus ν is independent of the number of sensors.

The denominator of $\rho_{\mathrm{o,GLC}}$ is defined as $\gamma = \|\mathbf{R}_M - \nu\mathbf{I}_M\|^2$, which can be given by

$$\begin{aligned}\gamma &= \left\|\sum_{d=0}^{D-1}\sigma_d^2\mathbf{a}_d\mathbf{a}_d^H + \sigma_n^2\mathbf{I}_M - \left(\sum_{d=0}^{D-1}\sigma_d^2\mathbf{I}_M + \sigma_n^2\mathbf{I}_M\right)\right\|^2 \\ &= \left\|\sum_{d=0}^{D-1}\sigma_d^2(\mathbf{a}_d\mathbf{a}_d^H - \mathbf{I}_M)\right\|^2.\end{aligned} \tag{31}$$

If only focusing on one term in (31), we can get

$$\begin{aligned}\left\|\sigma_d^2\left(\mathbf{a}_d\mathbf{a}_d^H - \mathbf{I}_M\right)\right\|^2 &= \sigma_d^4\left\{\mathrm{tr}\left[(M-2)\mathbf{a}_d\mathbf{a}_d^H\right] + M\right\} \\ &= \sigma_d^4\left(M^2 - M\right),\end{aligned} \tag{32}$$

with $d = 0,\ldots,D-1$, so we can draw a conclusion that

$$\gamma = \mathcal{O}(M^2), \tag{33}$$

where $\mathcal{O}(\cdot)$ means "on the order of".

As for the parameter ε, we let $E_M = \|\widehat{\mathbf{R}}_M - \mathbf{R}_M\|$. As the truncation argument described in [39], for every $\delta > 0$, one has with probability at least $1-\delta$ that:

$$E_M \lesssim_{q,\delta} (\log\log M)^2\left(\frac{M}{N}\right)^{\frac{1}{2}-\frac{2}{q}}, \tag{34}$$

if the receiving signal satisfies the moment assumptions:

$$\|\mathbf{x}(n)\|_2 \le K\sqrt{M} \quad a.s., \tag{35}$$

$$(E|\langle\mathbf{x}(n),\mathbf{x}_0\rangle|^q)^{1/q} \le L \quad \forall\mathbf{x}_0 \in S^{M-1}, \tag{36}$$

for some K and L, with $4 \le M \le N$ and $q > 4$, where S^{M-1} denotes the unit Euclidean sphere in $\mathbb{R}^M$, $\langle\cdot\rangle$ denotes inner product, and inequality of the form $a \lesssim_{q,\delta} b$ means that $a \le C_{q,\delta}b$ where $C_{q,\delta}$ depends only on the parameters q, δ.

Because the boundedness assumptions (35) and (36) can be sufficed in the analysis of GLC [39], [40], assuming that the number of snapshots N is constant and large enough, and let

$$p = \frac{1}{2} - \frac{2}{q}, \tag{37}$$

then the parameter ε satisfies that

$$\varepsilon = \mathcal{O}(M^{2p}(\log\log M)^4), \tag{38}$$

where $0 < p < 1/2$ due to $q > 4$.

From (33) and (38), one can find that the order of magnitude of ε is much less than that of γ with high probability. Thus, $\rho_{\mathrm{o,GLC}}$ will decrease when the number of sensors M increases.

In order to study the behavior of the diagonal loading level of GLC intuitively, we give the variation curves of $\rho_{\mathrm{o,GLC}}$ when M increases from 10 to 100 with $N = 100$ and $N = 200$ in Fig. 1. Without loss of generality, we assume that there are three directional far-field narrowband signals impinging on a ULA from directions 0°, 30° and 45°, respectively. Regard the first signal as SOI, and the others are interferences. The power of SOI is 10dB and that of interferences

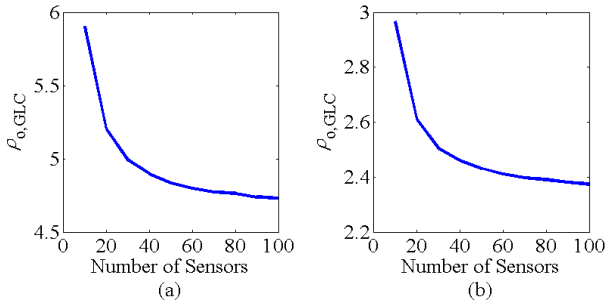

FIGURE 1. $\rho_{o,GLC}$ **versus the number of sensors** M**. (a)** $N = 100$**, (b)** $N = 200$**.**

are 20dB. In addition, there is spatially white complex Gaussian noise with zero-mean and power 0dB. For each scenario 1000 Monte-Carlo trials are performed. As can be seen from Fig. 1, when M increases from 10 to 100, the diagonal loading level of GLC will decrease. Comparing Fig. 1 (a) with (b), one can also find that the diagonal loading level of GLC will decrease as N increases.

From this study and previous studies, one can find that all the mentioned parameter-free RAB techniques will have performance degradation in the cases with a large number of snapshots or that of sensors, so a novel automatic diagonal loading method is expected which can perform well in the two limiting cases.

V. PROPOSED NRP-TMMSE METHOD

To solve the problem that the diagonal loading level of GLC declines when the number of sensors increases, this section introduces a noise reduction preprocessing into a truncated minimum mean square error criterion (NRP-TMMSE), where the TMMSE criterion can be given by

$$\min_{\alpha_t,\beta_t}\left\{\mathrm{MSE}(\widetilde{\mathbf{R}}_t)\right\} = \min_{\alpha_t,\beta_t} E\left\{\|\alpha_t\widehat{\mathbf{R}}_t + \beta_t\mathbf{T}_t - \mathbf{R}_t\|^2\right\}, \quad (39)$$

where α_t and β_t are nonnegative shrinkage parameters. $\widetilde{\mathbf{R}}_t$, $\widehat{\mathbf{R}}_t$ and $\mathbf{R}_t$ are the estimated, the sample and the true covariance matrix of target-plus-interference signal of $\mathbf{x}(n)$, respectively. $\mathbf{T}_t$ is an $M \times M$ matrix that can be constructed by the eigenvectors of $\widehat{\mathbf{R}}_t$. By solving (39), we can obtain the parameters $\hat{\alpha}_t$ and $\hat{\beta}_t$, thus the estimate covariance matrix can be expressed as

$$\widetilde{\mathbf{R}}_{\mathrm{NRP-TMMSE}} = \hat{\alpha}_t\widehat{\mathbf{R}}_x + \hat{\beta}_t\mathbf{I}. \quad (40)$$

There are two critical issues in NRP-TMMSE, one is to estimate $\widetilde{\mathbf{R}}_t$ and the other is to construct the matrix $\mathbf{T}_t$.

Note that both (39) and (17) use the MMSE criterion to estimate the covariance matrix in an optimal way. There are two obvious differences between (39) and (17). First, (39) only considers the true covariance matrix of the target-plus-interference signal, while (17) also considers the noise covariance matrix. Second, (17) use the identity matrix directly, while (39) uses a reconstructed matrix $\mathbf{T}_t$ instead, where $\mathbf{T}_t$ relates the estimate covariance matrix of the target-plus-interference signal.

A. NOISE REDUCTION PREPROCESSING

We utilize two conventional methods to reduce the noise of $\mathbf{x}(n)$. One is the least-square-estimate (LSE) method [34], in which the received noisy signal of the mth sensor is denoted as $\mathbf{x}_m = [x_m(0), x_m(1), \ldots, x_m(N-1)]^T$ $(m = 0, 1, \ldots, M-1)$. Then we construct an $N_1 \times N_2$ Hankel matrix of $\mathbf{x}_m$ as [34]:

$$\mathbf{H}^{(m)} = \begin{bmatrix} x_m(0) & x_m(1) & \ldots & x_m(N_2-1) \\ x_m(1) & x_m(2) & \ldots & x_m(N_2) \\ \vdots & \vdots & \ddots & \vdots \\ x_m(N_1-1) & x_m(N_2) & \ldots & x_m(N-1) \end{bmatrix}, \quad (41)$$

where $N_1 + N_2 = N + 1$ and $N_1 \geq N_2$. As shown in [34], $\mathbf{H}^{(m)}$ can be written as

$$\mathbf{H}^{(m)} = \mathbf{H}_{ti}^{(m)} + \mathbf{H}_n^{(m)}, \quad (42)$$

where $\mathbf{H}_{ti}^{(m)}$ and $\mathbf{H}_n^{(m)}$ are the Hankel matrixes derived form the target-plus-interference signal and the white complex Gaussian noise signal, respectively. In addition, $\mathrm{rank}(\mathbf{H}_{ti}^{(m)}) = D < N_2$, and $\mathrm{rank}(\mathbf{H}^{(m)}) = \mathrm{rank}(\mathbf{H}_n^{(m)}) = N_2$. If the number of the signals is estimated as D_0, and the number of snapshots is large enough, then we can let $N_2 = 2\,D_0$.

The singular value decomposition (SVD) of $\mathbf{H}^{(m)}$ can be given by

$$\mathbf{H}^{(m)} = \mathbf{G}\Sigma\mathbf{P}^H, \quad (43)$$

where the nonnegative diagonal elements of $\Sigma \in \mathbb{C}^{N_1\times N_2}$ are the singular values of $\mathbf{H}^{(m)}$, ranging in order from large to small, namely $\zeta_0 \geq \zeta_1 \cdots \geq \zeta_{N_2-1}$. The columns of $\mathbf{G} \in \mathbb{C}^{N_1\times N_1}$ and $\mathbf{P} \in \mathbb{C}^{N_2\times N_2}$ are the left and right singular vectors of $\mathbf{H}^{(m)}$, respectively. The SVD of $\mathbf{H}^{(m)}$ can be divided as [34]

$$\mathbf{H}^{(m)} = [\mathbf{G}_1 \quad \mathbf{G}_2]\begin{bmatrix}\Sigma_1 & \mathbf{0} \\ \mathbf{0} & \Sigma_2\end{bmatrix}\begin{bmatrix}\mathbf{P}_1^T \\ \mathbf{P}_2^T\end{bmatrix}, \quad (44)$$

where, $\mathbf{G}_1 \in \mathbb{C}^{N_1\times D_0}$, $\Sigma_1 \in \mathbb{C}^{D_0\times D_0}$, and $\mathbf{P}_1 \in \mathbb{C}^{N_2\times D_0}$. The LSE of $\mathbf{H}_{ti}^{(m)}$ can be obtained as

$$\widehat{\mathbf{H}}_{ti}^{(m)} = \mathbf{G}_1\Sigma_1\mathbf{P}_1^H, \quad (45)$$

The denoised signal of the mth sensor $y_m(n)$ can be reconstructed by arithmetic averaging along the anti-diagonals of $\widehat{\mathbf{H}}_{ti}^{(m)}$:

$$y_m(n) = \frac{1}{\kappa - \iota + 1}\sum_{i=\iota}^{\kappa}\widehat{\mathbf{H}}_{ti}^{(m)}(n-i+2, i), \quad (46)$$

with,

$$\iota = \max(1, n - N_1 + 2), \quad (47)$$

$$\kappa = \min(N_2, n+1). \quad (48)$$

Accordingly, by repeating the process for each sensor, we can obtain the signal vector of the nth snapshot, namely

$\mathbf{y}_{\mathrm{LS}}(n) = [y_0(n), y_1(n), \ldots, y_{M-1}(n)]^T$. As the computational complexity of LSE method is $\mathcal{O}(M \cdot N^3)$, which is too high for implementation, we need to introduce a low-complexity noise reduction algorithm.

The multichannel wiener filtering (MWF) method can be a choice for reducing the computational complexity in noise reduction, the filtering process of which can be written as [35]

$$\mathbf{y}_{\mathrm{MWF}}(n) = \mathbf{W}_{\mathrm{MWF}}\, \mathbf{x}(n), \tag{49}$$

where

$$\mathbf{W}_{\mathrm{MWF}} = \widehat{\mathbf{R}}_x^{-1} \left(\widehat{\mathbf{R}}_x - \widehat{\mathbf{R}}_n \right), \tag{50}$$

is the estimated multichannel wiener filter, $\widehat{\mathbf{R}}_n$ is the estimate white noise covariance matrix. If the eigenvalue decomposition of $\widehat{\mathbf{R}}_x$ can be written as

$$\widehat{\mathbf{R}}_x = \mathbf{U}\widehat{\Gamma}\mathbf{U}^H, \tag{51}$$

where each column of matrix $\mathbf{U} \in \mathbb{C}^{M\times M}$ is the eigenvector of $\widehat{\mathbf{R}}_x$, and the elements of matrix $\widehat{\Gamma} = \mathrm{diag}(\hat{\tau}_0, \hat{\tau}_1, \ldots, \hat{\tau}_{M-1})$ are the eigenvalues of $\widehat{\mathbf{R}}_x$, then the noise covariance matrix can be estimated as

$$\widehat{\mathbf{R}}_n = \left(\frac{1}{M - D_0} \sum_{m=D_0}^{M-1} \hat{\tau}_m \right) \cdot \mathbf{I}. \tag{52}$$

Thus, by substituting (52) into (50), we can obtain the multichannel wiener filter. The computational complexity of MWF is $\mathcal{O}(M^2 \cdot N)$, which is much less than the LSE algorithm, especially when considering $N \gg M$ generally. For convenience, we unify the denoised signal $\mathbf{y}_{\mathrm{LS}}(n)$ and $\mathbf{y}_{\mathrm{MWF}}(n)$ as $\mathbf{y}(n)$ in what follows.

Algorithm 1 LS-TMMSE

1) **Conditions**
   a) Given the input signal vector of the mth sensor $\mathbf{x}_m(n)$.
   b) Estimate the number of directional sound sources D_0.
   c) Set the size of the Hankel matrix $\mathbf{H}^{(m)}$ as $N_1 \times N_2$.
2) **Computation**
   a) Noise reduction
      i) Construct the Hankel matrix $\mathbf{H}^{(m)}$ ($\mathbf{H}^{(m)} = \mathbf{H}_{ti}^{(m)} + \mathbf{H}_n^{(m)}$).
      ii) Calculate the SVD of $\mathbf{H}^{(m)}$ using (43).
      iii) Divide the SVD of $\mathbf{H}^{(m)}$ using (44), and Estimate the LSE of $\mathbf{H}_{ti}^{(m)}$.
      iv) Repeat the steps above for each sensor and reconstruct the denoised signal $\mathbf{y}(n)$.
      v) Calculate the estimated target-plus-interference covariance matrix $\widehat{\mathbf{R}}_t = \frac{1}{N}\sum_{n=1}^{N} \mathbf{y}(n)\mathbf{y}^H(n)$.
   b) Construction of $\mathbf{T}_t$
      i) Calculate the eigenvalue decomposition of $\widehat{\mathbf{R}}_t$.
      ii) Construct $\mathbf{T}_t$ by using (55).
   c) TMMSE criterion
      i) Solve equation (39), and obtain the parameters $\hat{\alpha}_t$ and $\hat{\beta}_t$.

B. CONSTRUCTION OF $\mathbf{T}_t$

Once we obtain the denoised signal $\mathbf{y}(n)$, the sample covariance matrix $\widehat{\mathbf{R}}_t$ can be calculated by

$$\widehat{\mathbf{R}}_t = \frac{1}{N} \sum_{n=1}^{N} \mathbf{y}(n)\mathbf{y}^H(n). \tag{53}$$

Algorithm 2 MWF-TMMSE

1) **Conditions**
   a) Given the sample covariance matrix of input signals $\widehat{\mathbf{R}}_x$.
   b) Estimate the number of directional sound sources D_0.
2) **Computation**
   a) Noise reduction
      i) Estimate the white noise covariance matrix $\widehat{\mathbf{R}}_n$ using (52).
      ii) Calculate the multichannel wiener filter $\mathbf{W}_{\mathrm{MWF}}$.
      iii) Obtain the denoised signal $\mathbf{y}$.
      v) Calculate the estimated target-plus-interference covariance matrix $\widehat{\mathbf{R}}_t = \frac{1}{N}\sum_{n=1}^{N} \mathbf{y}(n)\mathbf{y}^H(n)$.
   b) Construction of $\mathbf{T}_t$
      i) Calculate the eigenvalue decomposition of $\widehat{\mathbf{R}}_t$.
      ii) Construct $\mathbf{T}_t$ by using (55).
   c) TMMSE criterion
      i) Solve equation (39), and obtain the parameters $\hat{\alpha}_t$ and $\hat{\beta}_t$.

The eigenvalue decomposition of $\hat{\mathbf{R}}_t$ can be expressed as

$$\widehat{\mathbf{R}}_t = \mathbf{V}\widehat{\Xi}\mathbf{V}^H, \tag{54}$$

where each column of matrix $\mathbf{V} \in \mathbb{C}^{M\times M}$ is the eigenvector of $\widehat{\mathbf{R}}_t$. And the elements of $\widehat{\Xi} = \mathrm{diag}(\hat{x}_0, \hat{x}_1, \ldots, \hat{x}_{D-1}, \ldots, \hat{x}_{M-1})$ with $\hat{x}_0 \geq \hat{x}_1 \cdots \geq \hat{x}_{M-1} \geq 0$ are the eigenvalues of $\widehat{\mathbf{R}}_t$, which can be divided into two parts: $\hat{x}_i (i = 0, \ldots, D-1)$ corresponds to target-plus-interference power, and $\hat{x}_i (i = D, \ldots, M-1)$ corresponds to noise power. Then the matrix $\mathbf{T}_t$ can be constructed as

$$\mathbf{T}_t = \mathbf{V}\mathrm{diag}\left\{ \underbrace{1, 1, \ldots, 1}_{D_0}, 0, \ldots, 0 \right\} \mathbf{V}^H. \tag{55}$$

The solution of (39) can be obtained in a similar way to GLC:

$$\hat{\beta}_t = \min\left[\hat{\nu}_t \frac{\hat{\varepsilon}_t}{\left\| \widehat{\mathbf{R}}_t - \hat{\nu}_t \mathbf{T}_t \right\|^2},\ \hat{\nu}_t \right], \tag{56}$$

$$\hat{\alpha}_t = 1 - \frac{\hat{\beta}_t}{\hat{\nu}_t}, \tag{57}$$

where $\hat{\nu}_t = \mathrm{tr}(\widehat{\mathbf{R}}_t \mathbf{T}_t^H)/D_0$, and the value of $\hat{\varepsilon}_t$ can be estimated as

$$\hat{\varepsilon}_t = \frac{1}{N^2} \sum_{n=1}^{N} \|\mathbf{y}(n)\|^4 - \frac{1}{N} \left\| \widehat{\mathbf{R}}_t \right\|^2. \tag{58}$$

Accordingly, the weight vector of NRP-TMMSE can be expressed as (assuming that $\hat{\alpha}_t \neq 0$)

$$\mathbf{w}_{\mathrm{NRP-TMMSE}} = \frac{\left(\widehat{\mathbf{R}}_x + \frac{\hat{\beta}_t}{\hat{\alpha}_t}\mathbf{I} \right)^{-1} \mathbf{a}_0}{\mathbf{a}_0^H \left(\widehat{\mathbf{R}}_x + \frac{\hat{\beta}_t}{\hat{\alpha}_t}\mathbf{I} \right)^{-1} \mathbf{a}_0}. \tag{59}$$

As can be seen from (59), NRP-TMMSE also belongs to the diagonal loading method and its diagonal loading level is $\hat{\beta}_t/\hat{\alpha}_t$, we denote it as $\rho_{\mathrm{NRP-TMMSE}}$. The validation of the proposed method is given in Appendix A.

As mentioned above, NRP-TMMSE is a combination of noise reduction preprocessing and the TMMSE criterion, which can be denoted as LS-TMMSE and MWF-TMMSE according to its noise reduction algorithm. We summarize the implementation of the proposed LS-TMMSE and MWF-TMMSE in **Algorithm 1** and **Algorithm2**, respectively.

VI. STEERING VECTOR ESTIMATION

As the parameter-free RAB techniques such as HKB, GLC, SMF, LS-TMMSE, and MWF-TMMSE only consider estimating the covariance matrix, they are all sensitive to the DOA mismatch as well as the sensor position perturbations. To solve the problem, we construct a series connection between these RAB techniques and a well-known steering vector estimation (SVE) method given in [11]. Thus, they are denoted as HKB-SVE, GLC-SVE, SMF-SVE, LS-TMMSE-SVE and MWF-TMMSE-SVE, respectively.

The only prior information used in the SVE method is the imprecise knowledge of the angular sector Θ of the desired signal and array geometry. By introducing the following positive semi-definite matrix variable $\mathbf{Z} \triangleq \hat{\mathbf{a}}_0\hat{\mathbf{a}}_0^H$, the steering vector can be estimated using a convex optimization approach

$$\begin{aligned} \min_{\mathbf{Z}} \quad & \mathrm{tr}(\widehat{\mathbf{R}}_x^{-1}\mathbf{Z}) \\ \text{subject to} \quad & \mathrm{tr}(\mathbf{Z}) = M \\ & \mathrm{tr}(\widetilde{\mathbf{C}}\mathbf{Z}) \le \Delta_0 \\ & \mathbf{Z} \succeq \mathbf{0}, \end{aligned} \tag{60}$$

where $\widetilde{\mathbf{C}} \triangleq \int_{\widetilde{\Theta}} \mathbf{a}(\theta)\mathbf{a}^H(\theta)d\theta$, $\widetilde{\Theta}$ is the complement of the sector Θ, $\mathbf{a}(\theta)$ is the assumed steering vector with the direction of θ, and $\Delta_0 \triangleq \max_{\theta\in\Theta} \mathbf{a}^H(\theta)\widetilde{\mathbf{C}}\mathbf{a}(\theta)$. Because there is a high possibility of the rank-one solution for this optimization problem [11], the estimated steering vector $\hat{\mathbf{a}}_0$ can be calculated as the principal eigenvector of the positive semi-definite matrix $\mathbf{Z}$.

VII. NUMERICAL RESULTS

In this section, we evaluate HKB, GLC, SMF, QC, LS-TMMSE and MWF-TMMSE algorithms through simulations. A ULA with $M = 20$ elements is adopted in the test. Suppose that $D = 4$, and the temporally white complex Gaussian far-field narrowband signals impinge on the ULA from directions 0°, 30°, 45°, and 60°, respectively. We regard the first signal as the SOI with power 10dB, and the remaining signals as interferences with power 20dB. The noise is spatially and temporally white complex Gaussian process with zero-mean and power 0dB. In the following examinations, the output SINR is calculated by substituting the optimized weight vector for $\mathbf{w}_{\mathrm{SCB}}$ in (8). In the following scenarios, two conditions are considered. In the first condition, the steering vector of SOI is accurately known. In the second condition, that steering vector of SOI is imprecise because of the DOA error and the sensor position perturbations, where the DOA error is assumed to be random and uniformly distributed in $[-5°, 5°]$ and the sensor position perturbations are uniformly drawn from $[-0.05, 0.05]$. Particularly, to satisfy the constraint in (27) and to simulate a realistic circumstance that the assumed uncertainty set is smaller than the real DOA mismatch, we set the DOA range of QC as $[-2°, 2°]$. For each scenario 1000 Monte-Carlo trials are performed.

A. THE IMPACT OF INACCURATE ESTIMATION OF THE SIGNAL NUMBERS

As mentioned above, in the implementation of NRP-TMMSE, we need to estimate the number of signal number. To examine how the estimation error affects the performance of NRP-TMMSE. Fig. 2 shows the averaged output SINRs of LS-TMMSE and MWF-TMMSE versus the number of snapshots N as $D_0 = 1, 4, 6, 10, 12$, respectively. As shown in Fig. 2 (a), we can observe that LS-TMMSE can achieve the optimal performance as $D_0 = D = 4$, and it is not very sensitive to the inaccurate estimation of the number of the sources. When $D_0 > D$, the performance of LS-TMMSE degrades as the estimation error increases. And when $D_0 = 1$, the performance of LS-TMMSE is very close to the optimal one. We may draw an extra conclusion that we'd better underestimate the number of sound sources rather than overestimate it when applying the proposed LS-TMMSE. As shown in Fig. 2 (b), the estimation error can barely affect the performance of MWF-TMMSE. As a consequence, when using NRP-TMMSE, we only need a rough estimated number of directional signals,

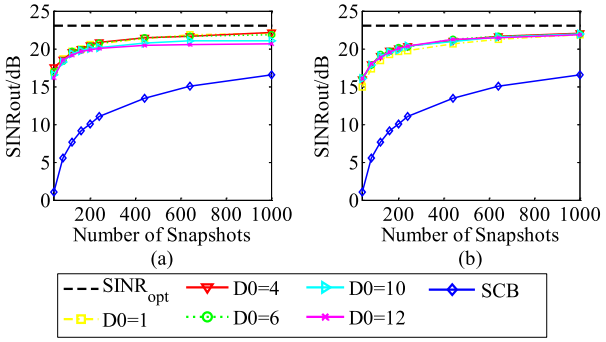

FIGURE 2. Beamformer output SINR versus N for different values of D_0 using NRP-TMMSE. (a) The output SINR of LS-TMMSE. (b) The output SINR of MWF-TMMSE.

B. THE IMPACT OF THE NUMBER OF SNAPSHOTS

Then, we examine the diagonal loading level of each beamformer as the number of snapshots N increases, assuming that the steering vector of SOI and the number of signals are precisely known. Fig. 3 show the mean value of the diagonal loading levels of HKB, GLC, SMF, QC, LS-TMMSE and MWF-TMMSE, respectively. One can find that the diagonal loading levels of GLC and NRP-TMMSE decrease, but the diagonal loading level of HKB increases contrarily, as N increases. At the meanwhile, the diagonal loading levels of SMF and QC tend to be a constant. In addition, we note

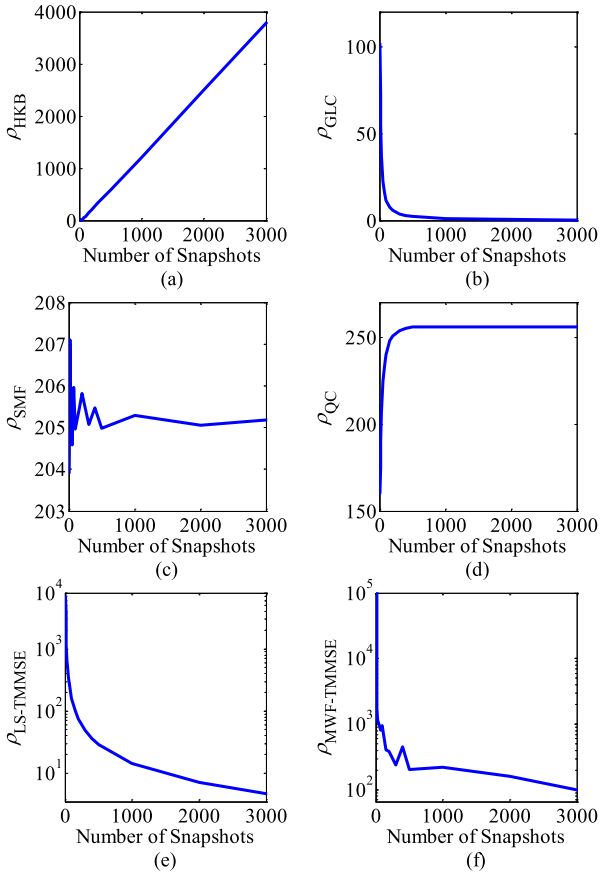

FIGURE 3. Comparison of average diagonal loading levels versus N with $M = 20$. (a) ρ_{HKB}. (b) ρ_{GLC}. (c) ρ_{SMF}. (d) ρ_{QC}. (e) $\rho_{LS-TMMSE}$. (f) $\rho_{MWF-TMMSE}$.

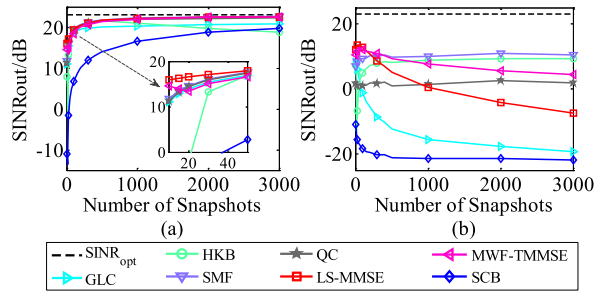

FIGURE 4. Output SINRs of the original RAB techniques versus N with $M = 20$. (a) In the absence of mismatch. (b) In the presence of mismatch.

that the diagonal loading level of NRP-TMMSE is larger than those of GLC , SMF and QC, especially the MWF-TMMSE. Among the four diagonal loading methods, the diagonal loading level of GLC is the smallest one.

To analyze how the diagonal loading levels affect the performances of the considered beamformers, Fig. 4 shows the mean output SINRs of the mentioned RAB techiques versus the number of snapshots N, where Fig. 4 (a) presents the circumstance that the steering vector is accurately known, and Fig. 4 (b) presents the circumstance that there exists steering vector mismatch. As shown in Fig. 4 (a), the output SINRs of all diagonal loading methods are larger than SCB. The output SINR of HKB decreases when N exceeds about 440 in this example. When N is larger than 2500, the performance of HKB will be even worse than SCB. This is because the diagonal loading level of HKB, as shown in Fig. 3 (a), grows from a small value to a very large value as N increases. Comparing the proposed algorithms to GLC, we note that their output SINRs are close to each other when N is less than 200, but the proposed algorithms are better than GLC as N increases. As for the SMF and QC, their convergence rates are as fast as the proposed algorithms. By local amplification, we note that when the number of snapshots is very small, ie., N is equal or twice as large as M or even smaller than M, the output SINR of LS-TMMSE is the largest. This is because the diagonal loading level of LS-TMMSE is large enough to improve the convergence rate. However, the larger diagonal loading level is not always the better choice. The diagonal loading level of MWF-TMMSE is up to 10^5 when N is around 20, but its performance is relatively worse than LS-TMMSE, SMF, and QC. From Fig. 4 (b), we note that when there exists steering vector mismatch, all the RAB techniques have a severely performance degradation, where the curves of GLC, LS-TMMSE and MWF-TMMSE drop more seriously than SMF, QC and HKB. The reason is that, as N increases, the diagonal loading levels of GLC, LS-TMMSE and MWF-TMMSE decline to very small values, which are not enough to guarantee the robustness of them to the steering vector mismatch.

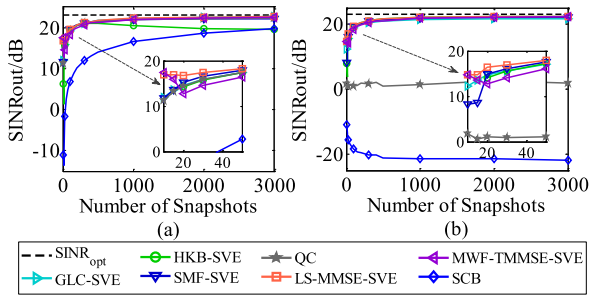

FIGURE 5. Output SINRs of the series connection structure between RAB techniques and SVE algorithm versus N with $M = 20$. (a) In the absence of mismatch. (b) In the presence of mismatch.

To examine the effect of the SVE algorithm, Fig. 5 shows the mean output SINRs of the series connection structure between the RAB techniques and the SVE algorithm versus N, where Fig. 5 (a) presents the circumstance that the steering vector is accurately known, while Fig. 5 (b) presents the circumstance that there exists steering vector mismatch. By comparing Fig. 4 (a) and Fig. 5 (a), we note that SVE improves the performance of GLC, which can be explained as that the covariance matrix deviation caused by the small number of snapshots is somewhat equal to the steering vector mismatch in terms of output SINR, and SVE can correct this mismatch. However, HKB-SVE has a poor

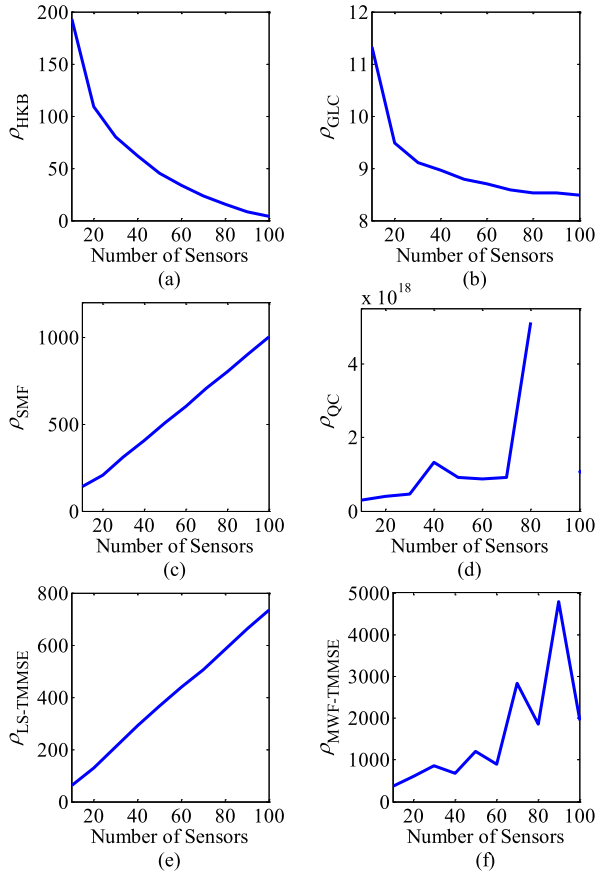

FIGURE 6. Comparison of average diagonal loading levels versus M with $N = 120$. (a) ρ_{HKB}. (b) ρ_{GLC}. (c) ρ_{SMF}. (d) ρ_{QC}. (e) $\rho_{LS-TMMSE}$. (f) $\rho_{MWF-TMMSE}$.

performance as N increases. This is because the SVE algorithm make the diagonal loading level of HKB more redundant. As shown in Fig. 5 (b), we can see that the series connection structure between the RAB techniques and SVE algorithm improves the robustness of those techniques remarkably. By locally magnify Fig. 5 (a) and Fig. 5 (b), we note that LS-TMMSE outperform other beamformers, especially when the number of snapshots is very small, i.e., less than 40. In addition, in the Fig. 4 (b) and Fig. 5 (b), the output SINR of QC is very small, which is due to that the real DOA range is larger than the assumed DOA range of QC.

C. THE IMPACT OF THE NUMBER OF SENSORS

Next, we examine the diagonal loading level of each beamformer as the number of sensors M increases without any steering vector mismatch, which is shown in Fig. 6. In this case, we set the snapshot number N equal to 120. In addition, to satisfy the constraint of QC given in (27), we let the uncertainty range of DOA to be $|\sin\theta_2 - \sin\theta_1| = \lambda/dM$, i.e., $\theta_2 = \arcsin(1/M)$, and $\theta_1 = -\arcsin(1/M)$. From Fig. 6, we observe that both the diagonal loading levels of GLC and HKB decrease as M increases. Whereas, the diagonal loading levels of SMF, QC, LS-TMMSE and

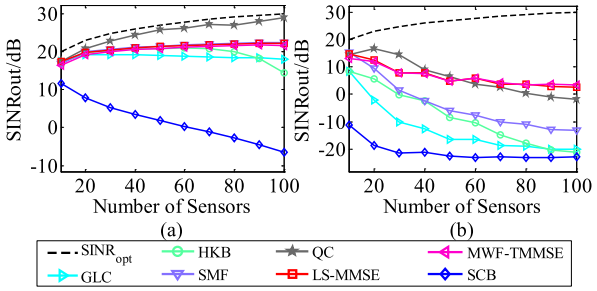

FIGURE 7. Output SINRs of the original RAB techniques versus M with $N = 120$. (a) In the absence of mismatch. (b) In the presence of mismatch.

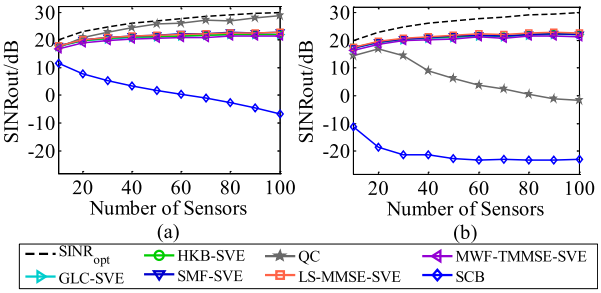

FIGURE 8. Output SINRs of the series connection structure between RAB techniques and SVE algorithm versus M with $N = 120$. (a) In the absence of mismatch. (b) In the presence of mismatch.

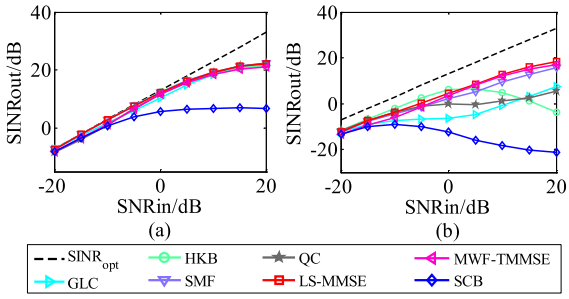

FIGURE 9. Output SINRs of the original RAB techniques versus input SNR with $N = 120$, $M = 20$. (a) In the absence of mismatch. (b) In the presence of mismatch.

MWF-TMMSE have the same variation tendency with M. Among them the diagonal loading level of QC can be much larger than other methods when M is larger than 70.

Fig. 7 shows the mean output SINRs of the original RAB techniques versus the number of sensors M, where Fig. 7 (a) considers the circumstance that the steering vector is accurately known, and Fig. 7 (b) takes into account the steering vector mismatch. In this examination, N is set to be 120. As shown in Fig. 7, if the input signal-to-noise ratio is given as $\mathrm{SNR_{in}}$, then the optimal output SINR will be estimated as $\mathrm{SINR_{opt}(dB)} \approx \mathrm{SNR_{in}(dB)} + 10\lg M$. Therefore, when $\mathrm{SNR_{in}}$ is constant, $\mathrm{SINR_{opt}}$ will increase in logarithmic form as M increases. The performance of SCB has serious degradation in Fig. 7 (a), which is due to the growing deviation between the sample covariance matrix $\widehat{\mathbf{R}}_x$ and the true covariance matrix $\mathbf{R}_x$ as M increases. Moreover, from

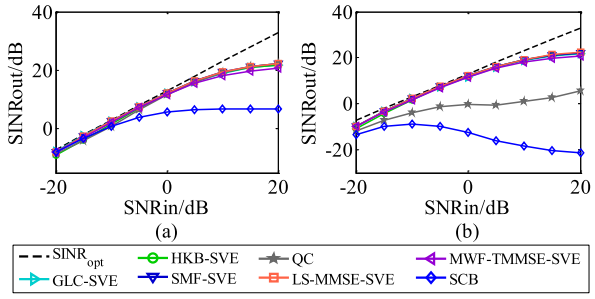

FIGURE 10. Output SINRs of the series connection structure between RAB techniques and SVE algorithm versus input SNR with $N = 120$, $M = 20$. (a) In the absence of mismatch. (b) In the presence of mismatch.

Fig. 7 (a), we note that the performance of HKB is worse than LS-TMMSE, MWF-TMMSE, SMF, and QC, especially when M exceeds 80. This is because of the decreasing diagonal loading level of HKB, as shown in Fig. 6 (a). However, the curve of GLC declines with the increasing M. The reasons account for the behavior are the declining trend of diagonal loading level of GLC and the whole value of diagonal loading level is very small. Therefore, GLC is somewhat sensitive to the number of sensors M. We note that the output SINR of QC is the closest to the optimal value. The reason is that when the deviation between $\widehat{\mathbf{R}}_x$ and $\mathbf{R}_x$ get larger as M increases, the diagonal loading level of QC appears a exponential growth trend in the iterative procedure. In particular, when $M = 80$, the diagonal loading level of QC can reach 5×10^{18}, which can effectively compensate the covariance matrix deviation. However, as the desired uncertainty range of DOA is becoming smaller with an increasing M, QC is not robust to the steering vector errors. As shown in Fig. 7 (b), the performance of all the RAB techniques have great degradation because of the steering vector mismatch. Among them, LS-TMMSE and MWF-TMMSE seem to be the most robust methods. This is because the diagonal loading levels of LS-TMMSE and MWF-TMMSE are relatively large when N is equal to 120.

Fig. 8 shows the mean output SINRs of the series connection structure between the RAB techniques and SVE algorithm versus the number of sensors M ($N = 120$), where Fig. 8 (a) considers the circumstance that the steering vector is accurately known, and Fig. 8 (b) takes into account the steering vector mismatch. Interestingly, by comparing Fig. 7 (a) with Fig. 8 (a), one can find that when combining with SVE algorithm, the performance of HKB and GLC will become better. The reason is the same with the improvement of the performance of GLC-SVE compared to GLC in terms of increasing N. As shown in Fig. 8 (b), the series connection structure between RAB techniques and SVE is highly robust to the steering vector mismatch, which has been verified in Fig. 5.

D. THE IMPACT OF INPUT SNR

In this part, we examine the performance of the beamformers as a function of the input SNR. The number of snapshots is fixed at 120. Fig. 9 (a) and Fig. 9 (b) show the output SINRs of the original RAB techiques versus the input SNR in the absence and in the presence of the steering vector mismatch, respectively. Fig. 9 (a) reveals that when the true steering vector is known, all the RAB techniques have the similar performance to each other, except the SCB. When there exists steering vector mismatch, as shown in Fig. 9 (b), the GLC, HKB, QC and SCB method have poor performance, especially the input SNR is greater than 0 dB. And the LS-TMMSE provides the best performance followed by the MWF-TMMSE.

Fig. 10 (a) and Fig. 10 (b) show the output SINRs of the series connection structure between the RAB techniques and the SVE algorithm versus input SNR in the absence and in the presence of the streeing vector mismatch, respectively. Comparing Fig. 9 (b) and 10 (b), we know that when connected with the SVE algorithm, those RAB techniques can be robust against the increasing input SNR and steering vector mismatch.

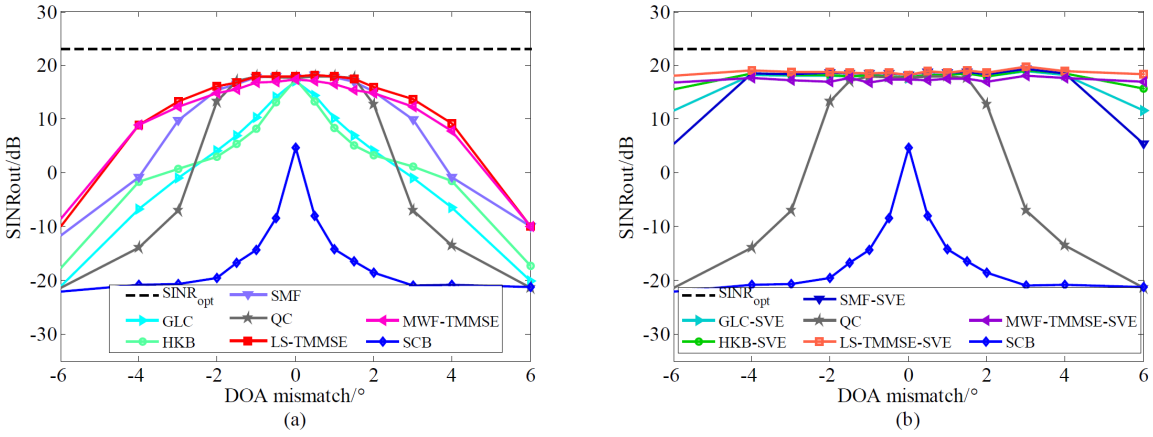

FIGURE 11. Beamformer output SINR with respect to the DOA angle mismatch. (a) Output SINRs of the original RAB techinques. (b) Output SINRs of the series connection structure between the RAB techinques and SVE algorithm.

E. THE IMPACT OF DOA ANGLE ERRORS

To further examine how the steering vector mismatch affect the performance of those RAB techniques, Fig. 11 shows the mean output SINRs with respect to the DOA angle errors, where N is set to 60, and M is set to 20. Fig. 11 (a) and Fig. 11 (b) show the performance of the original RAB techniques and the series connection structure, respectively. As shown in Fig. 11 (a), we note that LS-TMMSE is the most robust technique to the DOA angle mismatch, even without the series connection structure with the SVE algorithm. Its performance is followed by the MWF-TMMSE. This is because when the number of snapshots is equal to 60, the diagonal loading levels of LS-TMMSE and MWF-TMMSE are much larger than other RAB techniques. If constructing the series connection between these RAB techniques with the SVE algorithm, as shown in Fig. 11 (b), the robustness of these techniques are improved remarkably. Among them, LS-TMMSE-SVE and MWF-TMMSE-SVE are the most robust ones.

VIII. CONCLUSION

In this paper, we have asymptotically analyzed several parameter-free RAB techniques such as HKB, GLC, SMF and QC, and find that the performances of these conventional RAB techniques have different levels of degradation when the number of snapshots and that of sensors are relatively large, i.e., the number of sensors is from tens to hundreds times as many as the directional signals and the number of snapshots is from hundreds to thousands times as many as the number of sensors. To solve this problem, we emphatically study the problem of GLC, the performance of which may degrade with an increasing number of sensors, and propose the NRP-TMMSE algorithm which reduces the impact of number of sensors on the MMSE criterion by combining LSE-based or MWF-based noise reduction preprocessing with truncated MMSE criterion. Meanwhile, to improve the robustness of these RAB techniques against the steering vector mismatch, including the DOA errors and the sensor position perturbations, a series connection structure of RAB techniques and SVE algorithm is presented. A large number of simulations have been used to evaluate the performance of the proposed algorithm. It has been demonstrated that the diagonal loading level of NRP-TMMSE varies reasonably with varying number of snapshots and that of sensors, which makes it robust in all the cases, especially when the number of sensors is large, and the number of snapshots is very small, i.e., less than twice as many as the number of sensors. The simulations also verify that the series connection structure of RAB techniques and SVE algorithm is very robust to the steering vector mismatch. Moreover, the performance of NRP-TMMSE will barely be affected by the estimation error of the signal number. Thus, in the implementation of this method, the signal number is not the necessary prior knowledge, where it only needs to be roughly estimated according to the input signals.

APPENDIX A
VALIDATION OF THE PROPOSED METHOD

To validate the proposed method, the diagonal loading level of it is analyzed herein when the number of sensor approaches infinity.

As the theoretical diagonal loading level of GLC is given in (28), the theoretical diagonal loading level of NRP-TMMSE can be defined in a similar way, given by

$$\rho_{\mathrm{o,NRP-TMMSE}} = \nu_t \frac{\varepsilon_t}{\gamma_t}, \tag{61}$$

where, $\nu_t = \mathrm{tr}(\mathbf{R}_t\mathbf{T}_t^H)/D_0$, $\gamma_t = \|\nu_t\mathbf{T}_t - \mathbf{R}_t\|^2$, and $\varepsilon_t = E\{\|\widehat{\mathbf{R}}_t - \mathbf{R}_t\|^2\}$. In the following, we will analyze the diagonal loading level of NRP-TMMSE by means of calculating the order of the three parameters in (61) as a function of M.

Note that if the noise portion of the signal $\mathbf{x}(n)$ has been reduced completely, then the true covariance matrix $\mathbf{R}_t$ of the denoised signal $\mathbf{y}(n)$ can be written as

$$\mathbf{R}_t = \sum_{d=0}^{D-1} \sigma_d^2 \mathbf{a}_d \mathbf{a}_d^H. \tag{62}$$

According to the Cauchy-Schwarz inequality, the parameter ν_t can be calculated as

$$\begin{aligned}\nu_t &= \frac{\mathrm{tr}\left(\mathbf{R}_t\mathbf{T}_t^H\right)}{D_0} \\ &= \frac{\mathrm{tr}\left(\sum_{d=0}^{D-1}\sigma_d^2\mathbf{a}_d\mathbf{a}_d^H\mathbf{T}_t^H\right)}{D_0} \\ &\le \frac{MD_0\sum_{d=0}^{D-1}\sigma_d^2}{D_0} \\ &= M\sum_{d=0}^{D-1}\sigma_d^2,\end{aligned} \tag{63}$$

therefore, when $M \to \infty$, the parameter ν_t satisfies that

$$\nu_t = \mathcal{O}(M). \tag{64}$$

In practice, ν_t is the mean of the first D_0 eigenvalues of $\mathbf{R}_t$.

The parameter γ_t can be expressed as

$$\begin{aligned}\gamma_t &= \|\mathbf{R}_t - \nu_t\mathbf{T}_t\|^2 \\ &= \|\mathbf{R}_t\|^2 - D_0\nu_t^2,\end{aligned} \tag{65}$$

where,

$$\|\mathbf{R}_t\|^2 = \sum_{i=0}^{D-1}\sum_{j=0}^{D-1}\sigma_i^2\sigma_j^2(\mathbf{a}_i\mathbf{a}_i^H)(\mathbf{a}_j\mathbf{a}_j^H) = \mathcal{O}(M^2). \tag{66}$$

Since $\gamma_t \ge 0$, it is obvious that

$$\gamma_t = \mathcal{O}(M^f), \tag{67}$$

where $f \le 2$.

As for the parameter ε_t, we let $E_t = \|\widehat{\mathbf{R}}_t - \mathbf{R}_t\|$, it is obvious that E_t is of the same form with E_M, so E_t also satisfies the inequality (34). Accordingly, the order of ε and that of ε_t as a function of M are similar with each other, we can obtain that

$$\varepsilon_t = \mathcal{O}(M^{2p}(\log\log M)^4). \tag{68}$$

Specifically, if the number of snapshots is large enough, it is feasible to choose $q > 8$ in the boundedness assumptions (36) [39], then p will satisfies $1/4 < p < 1/2$. Since $M^{1/2} < (\log\log M)^4 < M$, we can conclude that

$$M < M^{2p}(\log\log M)^4 < M^{3/2}. \tag{69}$$

Finally, by substituting (64), (67), and (68) into (61), we can draw a conclude that when M increases, the diagonal loading level of NRP-TMMSE increases too, i.e., the tendency of the diagonal loading level of NRP-TMMSE with an increasing M coincides with the theoretical expected result. Therefore, NPR-TMMSE will outperform GLC when M approaches a large value (about from tens to hundreds times as many as the number of directional signals).

REFERENCES

[1] J. Capon, "High-resolution frequency-wavenumber spectrum analysis," *Proc. IEEE*, vol. 57, no. 8, pp. 1408–1418, Aug. 1969.
[2] H. Cox, R. Zeskind, and M. Owen, "Robust adaptive beamforming," *IEEE Trans. Acoust., Speech, Signal Process.*, vol. 35, no. 10, pp. 1365–1376, Oct. 1987.
[3] B. D. Carlson, "Covariance matrix estimation errors and diagonal loading in adaptive arrays," *IEEE Trans. Aerosp. Electron. Syst.*, vol. 24, no. 4, pp. 397–401, Jul. 1988.
[4] M. Rübsamen and A. B. Gershman, "Robust adaptive beamforming using multidimensional covariance fitting," *IEEE Trans. Signal Process.*, vol. 60, no. 2, pp. 740–753, Feb. 2012.
[5] S. A. Vorobyov, "Principles of minimum variance robust adaptive beamforming design," *Signal Process.*, vol. 93, no. 12, pp. 3264–3277, 2013.
[6] J. Li, P. Stoica, and Z. Wang, "On robust Capon beamforming and diagonal loading," *IEEE Trans. Signal Process.*, vol. 51, no. 7, pp. 1702–1715, Jul. 2003.
[7] S. A. Vorobyov, A. B. Gershman, and Z.-Q. Luo, "Robust adaptive beamforming using worst-case performance optimization: A solution to the signal mismatch problem," *IEEE Trans. Signal Process.*, vol. 51, no. 2, pp. 313–324, Feb. 2003.
[8] X. Jiang, W.-J. Zeng, A. Yasotharan, H. C. So, and T. Kirubarajan, "Robust beamforming by linear programming," *IEEE Trans. Signal Process.*, vol. 62, no. 7, pp. 1834–1849, Apr. 2014.
[9] X. Zhang, Q. Feng, N. Ge, and J. Lu, "Distributionally robust chance-constrained minimum variance beamforming," in *Proc. IEEE Int. Conf. Acoust., Speech Signal Process. (ICASSP)*, Mar. 2016, pp. 2881–2885.
[10] A. Hassanien, S. A. Vorobyov, and K. M. Wong, "Robust adaptive beamforming using sequential quadratic programming: An iterative solution to the mismatch problem," *IEEE Signal Process. Lett.*, vol. 15, pp. 733–736, Nov. 2008.
[11] A. Khabbazibasmenj, S. A. Vorobyov, and A. Hassanien, "Robust adaptive beamforming based on steering vector estimation with as little as possible prior information," *IEEE Trans. Signal Process.*, vol. 60, no. 6, pp. 2974–2987, Jun. 2012.
[12] F. Huang, W. Sheng, and X. Ma, "Modified projection approach for robust adaptive array beamforming," *Signal Process.*, vol. 92, no. 7, pp. 1758–1763, 2012.
[13] W. Jia, W. Jin, S. Zhou, and M. Yao, "Robust adaptive beamforming based on a new steering vector estimation algorithm," *Signal Process.*, vol. 93, no. 9, pp. 2539–2542, Sep. 2013.
[14] L. Huang, B. Zhang, and Z. Ye, "Robust adaptive beamforming using a new projection approach," in *Proc. IEEE Int. Conf. Digit. Signal Process. (DSP)*, Jul. 2015, pp. 1181–1185.
[15] Y. Gu and A. Leshem, "Robust adaptive beamforming based on interference covariance matrix reconstruction and steering vector estimation," *IEEE Trans. Signal Process.*, vol. 60, no. 7, pp. 3881–3885, Jul. 2012.
[16] L. Huang, J. Zhang, X. Xu, and Z. Ye, "Robust adaptive beamforming with a novel interference-plus-noise covariance matrix reconstruction method," *IEEE Trans. Signal Process.*, vol. 63, no. 7, pp. 1643–1650, Apr. 2015.
[17] Z. Zhang, W. Liu, W. Leng, A. Wang, and H. Shi, "Interference-plus-noise covariance matrix reconstruction via spatial power spectrum sampling for robust adaptive beamforming," *IEEE Signal Process. Lett.*, vol. 23, no. 1, pp. 121–125, Jan. 2016.
[18] Y. Wang, Q. Bao, and Z. Chen, "Robust adaptive beamforming using IAA-based interference-plus-noise covariance matrix reconstruction," *Electron. Lett.*, vol. 52, no. 13, pp. 1185–1186, May 2016.
[19] A. E. Hoerl, R. W. Kannard, and K. F. Baldwin, "Ridge regression: Some simulations," *Commun. Statist.-Theory Methods*, vol. 4, no. 2, pp. 105–123, Jan. 1975.
[20] L. Du, J. Li, and P. Stoica, "Fully automatic computation of diagonal loading levels for robust adaptive beamforming," *IEEE Trans. Aerosp. Electron. Syst.*, vol. 46, no. 1, pp. 449–458, Jan. 2010.
[21] M. Zhang, A. Zhang, and Q. Yang, "Robust adaptive beamforming based on conjugate gradient algorithms," *IEEE Trans. Signal Process.*, vol. 64, no. 22, pp. 6046–6057, Nov. 2016.
[22] C. Y. Chen and P. P. Vaidyanathan, "Quadratically constrained beamforming robust against direction-of-arrival mismatch," *IEEE Trans. Signal Process.*, vol. 55, no. 8, pp. 4139–4150, Aug. 2007.
[23] Y. Selén, R. Abrahamsson, and P. Stoica, "Automatic robust adaptive beamforming via ridge regression," in *Proc. IEEE Int. Conf. Acoust., Speech Signal Process. (ICASSP)*, vol. 2. Apr. 2007, pp. 965–968.
[24] X. Zhu, J. Li, and P. Stoica, "Knowledge-aided space-time adaptive processing," *IEEE Trans. Aerosp. Electron. Syst.*, vol. 47, no. 2, pp. 1325–1336, Apr. 2011.
[25] P. Stoica, J. Li, X. Zhu, and J. R. Guerci, "On using *a priori* knowledge in space-time adaptive processing," *IEEE Trans. Signal Process.*, vol. 56, no. 6, pp. 2598–2602, Jun. 2008.
[26] C. Gong, L. Huang, D. Xu, and Z. Ye, "Knowledge-aided robust adaptive beamforming with small snapshots," *Electron. Lett.*, vol. 49, no. 20, pp. 1259–1261, Sep. 2013.
[27] P. Stoica, P. Babu, and J. Li, "SPICE: A sparse covariance-based estimation method for array processing," *IEEE Trans. Signal Process.*, vol. 59, no. 2, pp. 629–638, Feb. 2011.
[28] Z. Yang and L. Xie, "On gridless sparse methods for line spectral estimation from complete and incomplete data," *IEEE Trans. Signal Process.*, vol. 63, no. 12, pp. 3139–3153, Jun. 2015.
[29] J. Benesty, C. Jingdong, and I. Cohen, *Design of Circular Differential Microphone Arrays*. Berlin, Germany: Springer, 2015.
[30] S. Yan, "Optimal design of modal beamformers for circular arrays," *J. Acoust. Soc. Amer.*, vol. 138, no. 4, pp. 2140–2151, Oct. 2015.
[31] D. P. Jarrett, E. A. P. Habets, and P. A. Naylor, *Theory and Applications of Spherical Microphone Array Processing*. Berlin, Germany: Springer, 2017, pp. 113–139.
[32] S. Yan, H. Sun, U. P. Svensson, X. Ma, and J. M. Hovem, "Optimal modal beamforming for spherical microphone arrays," *IEEE Trans. Audio, Speech, Language Process.*, vol. 19, no. 2, pp. 361–371, Feb. 2011.
[33] M. Rahmani, M. H. Bastani, and S. Shahraini, "Two layers beamforming robust against direction-of-arrival mismatch," *IET Signal Process.*, vol. 8, no. 1, pp. 49–58, Feb. 2014.
[34] S. H. Jensen, P. C. Hansen, S. D. Hansen, and J. A. Sorensen, "Reduction of broad-band noise in speech by truncated QSVD," *IEEE Trans. Speech Audio Process.*, vol. 3, no. 6, pp. 439–448, Nov. 1995.
[35] S. Doclo and M. Moonen, "GSVD-based optimal filtering for single and multimicrophone speech enhancement," *IEEE Trans. Signal Process.*, vol. 50, no. 9, pp. 2230–2244, Sep. 2002.
[36] Y. Gu and A. Leshem, "Robust adaptive beamforming based on jointly estimating covariance matrix and steering vector," in *Proc. IEEE Int. Conf. Acoust., Speech Signal Process. (ICASSP)*, May 2011, pp. 2640–2643.
[37] H. L. Van Trees, *Optimum Array Processing*. New York, NY, USA: Wiley, 2002.
[38] S. T. Smith, "Covariance, subspace, and intrinsic Cramér–Rao bounds," *IEEE Trans. Signal Process.*, vol. 53, no. 5, pp. 1610–1630, May 2005.
[39] R. Vershynin, "How close is the sample covariance matrix to the actual covariance matrix," *J. Theor. Probab.*, vol. 25, no. 3, pp. 655–686, Sep. 2012.
[40] R. Vershynin, "Approximating the moments of marginals of high-dimensional distributions," *Ann. Probab.*, vol. 39, no. 4, pp. 1591–1606, 2011.

YUXUAN KE received the B.S. degree in electronic and information engineering from Harbin Engineering University, Harbin, China, in 2014. She is currently pursuing the Ph.D. degree with the Key Laboratory of Noise and Vibration Research, Institute of Acoustics, University of Chinese Academy of Sciences.

Her research interests include array signal processing and speech enhancement.

CHENGSHI ZHENG (M'11–SM'13) received the B.S. degree in electronic engineering and information science from the University of Science and Technology of China, Hefei, China, in 2004, and the Ph.D. degree in acoustics from the Institute of Acoustics, University of Chinese Academy of Sciences, Beijing, in 2009.

Since 2009, he has been with the Institute of Acoustics, Chinese Academy of Sciences, where he is currently an Associate Professor with the Key Laboratory of Noise and Vibration Research. From 2014 to 2015, he was a Visiting Scientist with the Chair of Multimedia Communications and Signal Processing, University of Erlangen-Nuremberg, Germany. His research interests include speech enhancement, microphone array signal processing, and spectral estimation. He is a member of the European Association for Signal Processing.

RENHUA PENG received the B.S. degree in electronic engineering and information science from the University of Science and Technology of China, Hefei, China, in 2010, and the Ph.D. degree from the Institute of Acoustics, University of Chinese Academy of Sciences, Beijing, in 2015.

His research interests include speech enhancement and audio signal processing.

XIAODONG LI received the B.S. degree from Nanjing University, Nanjing, China, in 1988, the M.Eng. degree from Harbin Engineering University, Harbin, China, in 1991, and the Ph.D. degree in physical acoustics from the Institute of Acoustics, University of Chinese Academy of Sciences (IACAS), Beijing, China, in 1995.

He was a Research Fellow with The Hong Kong Polytechnic University for a short period, where he was involved in active control of sound. He was appointed as an Assistant Professor with IACAS in 1997, where he became an Associate Professor in 1998 and a Professor in 2002, where he is currently an Associate Director with the Key Laboratory of Noise and Vibration Research. His research interests include acoustic signal processing, active control of sound and vibration, and engineering acoustics.